Enhanced conductance through side-coupled double quantum dots

R. Žitko[1] and J. Bonča[1,2]
[1]*J. Stefan Institute, SI-1000 Ljubljana, Slovenia*
[2]*Department of Physics, FMF, University of Ljubljana, SI-1000 Ljubljana, Slovenia*
(Received 20 October 2005; published 30 January 2006)

Conductance, on-site, and intersite charge fluctuations and spin correlations in the system of two side-coupled quantum dots are calculated using Wilson's numerical renormalization group (NRG) technique. We also show the spectral density calculated using the density-matrix NRG, which for some parameter ranges remedies inconsistencies of the conventional approach. By changing the gate voltage and the interdot tunneling rate, the system can be tuned to a nonconducting spin-singlet state, the usual Kondo regime with an odd number of electrons occupying the dots, the two-stage Kondo regime with two electrons, or a valence-fluctuating state associated with a Fano resonance. Analytical expressions for the width of the Kondo regime and the Kondo temperature are given. We also study the effect of unequal gate voltages and the stability of the two-stage Kondo effect with respect to such perturbations.

DOI: 10.1103/PhysRevB.73.035332 PACS number(s): 72.10.Fk, 72.15.Qm, 73.63.Kv

I. INTRODUCTION

The advances in microfabrication have enabled studies of transport through single as well as coupled quantum dots, where at very low temperatures Kondo physics and magnetic interactions play an important role. A double-dot system represents the simplest possible generalization of a single-dot system which has been extensively studied in the past. Recent experiments demonstrate that an extraordinary control over the physical properties of double dots can be achieved,[1–4] which enables direct experimental investigations of the competition between the Kondo effect and the exchange interaction between localized moments on the dots. One manifestation of this competition is a two-stage Kondo effect that has recently been predicted in multilevel quantum dot systems with explicit exchange interaction coupled to one or two conduction channels.[5,6] Experimentally, it manifests itself as a sharp drop in the conductance versus gate voltage $G(V_G)$ (Ref. 7) or as nonmonotonic dependence of the differential conductance versus drain-source voltage $dI/dV_{ds}(V_{ds})$ (Ref. 8).

Fano resonances, which occur due to interference when a discrete level is weakly coupled to a continuous band, were recently observed in experiments on rings with embedded quantum dots[9] and quantum wires with side-coupled dots.[10] The interplay between Fano and Kondo resonances was investigated using equation-of-motion[11,12] and slave-boson techniques.[13]

In this work we study a double quantum dot (DQD) in a side-coupled configuration (Fig. 1), connected to a single conduction-electron channel. Systems of this type were studied previously using a noncrossing approximation,[14] embedding technique,[15] and slave-boson mean-field theory.[13,16] Numerical renormalization group (NRG) calculations were also performed recently,[17] where only narrow regimes of enhanced conductance were found at low temperatures. We will show that when the interdot overlap is large, wide regimes of enhanced conductance as a function of gate-voltage exist at low temperatures due to the Kondo effect, separated by regimes where localized spins on DQD's are antiferromagnetically (AFM) coupled. Kondo temperatures T_K follow a prediction based on Schrieffer-Wolff transformation and poor-man's scaling. In the limit when the dot a is only weakly coupled, the system enters the "two-stage" Kondo regime,[17,18] where we again find a wide regime of enhanced conductivity under the condition that the high and low Kondo temperatures (T_K and T_K^0 respectively) be well separated and the temperature of the system T be in the interval $T_K^0 \ll T \ll T_K$.

II. MODEL AND METHOD

The Hamiltonian that we study reads

$$H = \delta_d(n_d - 1) + \delta_a(n_a - 1) - t_d \sum_\sigma (d_\sigma^\dagger a_\sigma + a_\sigma^\dagger d_\sigma) + \frac{U_d}{2}(n_d - 1)^2 + \frac{U_a}{2}(n_a - 1)^2 + \sum_{k\sigma} \epsilon_k c_{k\sigma}^\dagger c_{k\sigma} + \sum_{k\sigma} V_d(k)(c_{k\sigma}^\dagger d_\sigma + d_\sigma^\dagger c_{k\sigma}), \quad (1)$$

where $n_d = \Sigma_\sigma d_\sigma^\dagger d_\sigma$ and $n_a = \Sigma_\sigma a_\sigma^\dagger a_\sigma$. The operators $d_\sigma^\dagger$ and $a_\sigma^\dagger$ are creation operators for an electron with spin σ on site d or a. On-site energies of the dots are defined by $\epsilon = \delta - U/2$. For simplicity, we choose the on-site energies and Coulomb interactions to be equal on both dots, $\delta_a = \delta_d = \delta$ and $U_a = U_d = U$. Coupling between the dots is described by the interdot tunnel coupling t_d. Dot d couples to both leads with equal hopping t'. As it couples only to symmetric combinations of

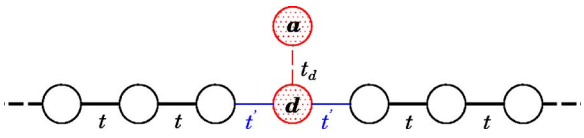

FIG. 1. (Color online) Side-coupled configuration of quantum dots.

the states from the left and right leads, we have used a unitary transformation[19] to describe the system as a variety of the single-channel, two-impurity Anderson model. The operator $c^\dagger_{k\sigma}$ creates a conduction band electron with momentum k, spin σ, and energy $\epsilon_k=-D\cos k$, where $D=2t$ is the half-bandwidth. The momentum-dependent hybridization function is $V_d(k)=-(2/\sqrt{N+1})t'\sin k$, where N in the normalization factor is the number of conduction band states.

We use the Meir-Wingreen formula for conductance in the case of proportionate coupling[20] which is known to apply under very general conditions (for example, the system need not be in a Fermi-liquid ground state) with spectral functions obtained using the NRG technique.[21–24] At zero temperature, the conductance is

$$G = G_0 \pi \Gamma \rho_d(0), \tag{2}$$

where $G_0=2e^2/h$, $\rho_d(\omega)$ is the local density of states of electrons on site d, and $\Gamma/D=(t'/t)^2$.

The NRG technique consists of logarithmic discretization of the conduction band, mapping onto a one-dimensional chain with exponentially decreasing hopping constants, and iterative diagonalization of the resulting Hamiltonian.[21] Only the low-energy part of the spectrum is kept after each iteration step; in our calculations we kept 1200 states, not counting spin degeneracies, using the discretization parameter $\Lambda=1.5$.

III. STRONG INTER-DOT COUPLING

A. Conductance and correlation functions

In Fig. 2(a) we present conductance through a double quantum dot at different values of interdot couplings versus δ. Due to the formation of Kondo correlations, conductance is enhanced, reaching the unitary limit in a wide range of δ.

To better understand multidot problems in the case of strong interdot coupling, it is helpful to exactly diagonalize the part of the Hamiltonian that describes the dots and rewrite the entire Hamiltonian [Eq. (1)] in a form similar to the ionic model:[25]

$$H_0 = \sum_{k,\sigma} \epsilon_k c^\dagger_{k,\sigma} c_{k,\sigma} + \sum_\alpha E(\alpha)|\alpha\rangle\langle\alpha|, \tag{3}$$

$$H_1 = \sum_{k,\sigma,\alpha,\beta} t_{k\sigma|\beta\to\alpha}|\alpha\rangle\langle\beta|c_{k,\sigma} + t^*_{k\sigma|\beta\to\alpha} c^\dagger_{k\sigma}|\beta\rangle\langle\alpha|, \tag{4}$$

where multi-indices α and β stand for quantum numbers (Q,S,S_z,r). Here Q is the charge number $Q=(n_a-1)+(n_d-1)$ and S and S_z are the spin and its component, while r numbers different states with the same Q,S,S_z quantum numbers. In the absence of a magnetic field, S_z is irrelevant and will be omitted from now on. Each (Q,S,r) multiplet is then $(2S+1)$-fold degenerate. Finally, the effective hopping coefficients

$$t_{k\sigma|\beta\to\alpha} = V_d(k)\langle\alpha|d^\dagger_\sigma|\beta\rangle \tag{5}$$

correspond to electrons hopping from the conduction band to the dots.

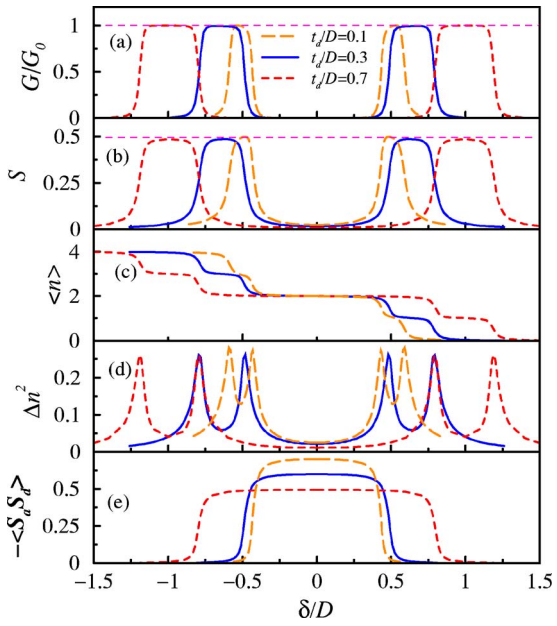

FIG. 2. (Color online) Conductance and correlation functions of DQD vs δ. Besides different values of t_d, indicated in the figure, other parameters of the model are $\Gamma/D=0.03$ and $U/D=1$. Temperature is $T/D=10^{-9}$, which for all parameters used corresponds to a zero-temperature limit. In particular, in the Kondo plateaus, $T \ll T_K$ for all δ.

The eigenvalue diagram in Fig. 3 represents the gate-voltage dependence of the multiplet energies $E(Q,S,r)$. From this diagram we can read off the ground state and the excited states for each parameter δ.

Regimes of enhanced conductance appear in the intervals approximately given by $\delta_1<|\delta|<\delta_2$, where $\delta_1=t_d(2\sqrt{1+(U/4t_d)^2}-1)$ and $\delta_2=(U/2+t_d)$. These estimates are obtained from the lowest energies of states with zero, one, and two electrons on the isolated double quantum dot:

$$E(-2,0,0) = U - 2\delta,$$

$$E\left(-1,\frac{1}{2},0\right) = U/2 - \delta - t_d,$$

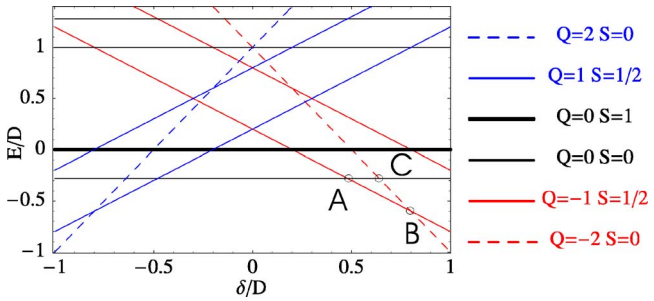

FIG. 3. (Color online) Eigenvalue diagram for the isolated DQD system. The diagram is symmetric, since for $\delta\to-\delta$, $E(Q,S,r)\to E(-Q,S,r)$. Points A and B correspond to valence-fluctuation regions when the charge on the dot changes, while point C corresponds to the center of the Kondo regime, when the Kondo temperature is the lowest. Parameters are $U/D=1$ and $t_d/D=0.3$.

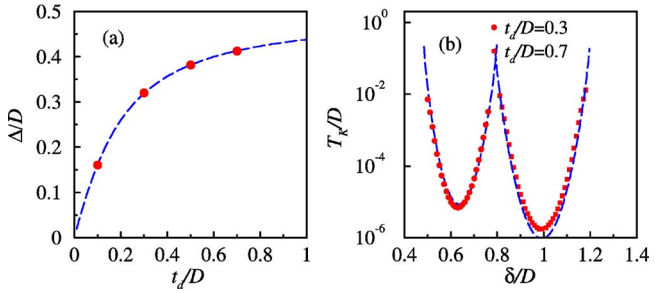

FIG. 4. (Color online) (a) The width of conductance peak Δ vs t_d as obtained from NRG calculations (solid circles), compared with the analytical result as given in the text (dashed line). (b) Kondo temperatures T_K vs δ as obtained from the widths of Kondo peaks (solid circles). The analytical estimate, Eq. (8), is shown using dashed lines. The rest of parameters are identical to those in Fig. 2.

$$E(0,0,0) = -2t_d\sqrt{1+(U/4t_d)^2} + U/2. \tag{6}$$

The widths of conductance peaks (measured at $G/G_0=1/2$) are therefore approximately given by

$$\Delta = U/2 + 2t_d[1-\sqrt{1+(U/4t_d)^2}]. \tag{7}$$

Note that in the limit of large t_d, $\Delta \simeq U/2$, and in the limit of large U, $\Delta \simeq 2t_d$. As it will become apparent later in this paper, this naive estimate fails when $t_d \to 0$. Comparison of conductance-peak widths with the analytical estimate Δ is shown in Fig. 4(a).

Next, we focus on various correlation functions. In Fig. 2(b) we show S, calculated from expectation value $\langle \mathbf{S}_{\rm tot}^2 \rangle = S(S+1)$, where $\mathbf{S}_{\rm tot}=\mathbf{S}_a+\mathbf{S}_d$ is the total spin operator. S reaches value $1/2$ in the regime where $G/G_0=1$. Enhanced conductance is thus followed by the local moment formation, indicative of the Kondo effect. This is further supported by the average double-dot occupancy $\langle n \rangle$, where $n=n_a+n_d$, which in the regime of enhanced conductivity approaches odd-integer values—i.e., $\langle n \rangle = 1$ and 3 [see Fig. 2(c)]. Transitions between regimes of nearly integer occupancies are rather sharp; they are visible as regions of enhanced charge fluctuations measured by $\Delta n^2 = \langle n^2 \rangle - \langle n \rangle^2$, as shown in Fig. 2(d). Finally, we show in Fig. 2(e) the spin-spin correlation function $\langle \mathbf{S}_a \cdot \mathbf{S}_d \rangle$. Its value is negative between two separated Kondo regimes where the conductance approaches zero—i.e., for $-\delta_1 < \delta < \delta_1$; otherwise, it is zero. This regime further coincides with $\langle n \rangle \sim 2$. Each dot thus becomes nearly singly occupied, and spins on the two dots form a local singlet due to effective exchange coupling $J_{\rm eff} \approx 4t_d^2/U$. Surprisingly, the absolute value of $\langle \mathbf{S}_a \cdot \mathbf{S}_d \rangle$ increases and it nearly reaches its limiting value—i.e., $\langle \mathbf{S}_a \cdot \mathbf{S}_d \rangle = -3/4$—as the inter-dot hopping t_d and, with it, $J_{\rm eff}$ decrease. This seeming contradiction is resolved by recognizing that $J_{\rm eff}$ represents the exchange interaction based on the effective Heisenberg coupling between localized spins on DQD's only in the limit when $t_d/U \to 0$. Smaller absolute values of $\langle \mathbf{S}_a \cdot \mathbf{S}_d \rangle$ are thus due to a small amount of double occupancy at larger values of t_d/U.

In Fig. 4(b) we present Kondo temperatures T_K vs δ extracted from the widths of Kondo peaks. Numerical results in the regime where $\langle n \rangle \sim 1$ and 3 fit the analytical expression obtained using the Schrieffer-Wolff transformation that leads to an effective single $S=1/2$ Kondo model. We obtain

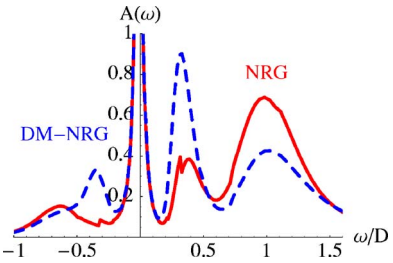

FIG. 5. (Color online) Comparison of spectral densities computed by the conventional NRG and by the density-matrix NRG technique for parameters where the conventional NRG approach has difficulties: $t_d/D=0.3$, $U/D=1$, $\Gamma/D=0.03$, and $\delta/D=0.48$. Note the discontinuities in the spectral density calculated using the conventional NRG. At low frequencies both method produce identical results, so we do not show the Kondo peak which exceeds the vertical scale of the plot. In this calculations, the effective temperature is zero.

$$T_K = 0.182U\sqrt{\rho_0 J}\exp[-1/\rho_0 J], \tag{8}$$

with

$$\rho_0 J = \frac{2\Gamma}{\pi}\left(\frac{\alpha}{\left|E\left(-1,\frac{1}{2},0\right)-E(-2,0,0)\right|} + \frac{\beta}{\left|E\left(-1,\frac{1}{2},0\right)-E(0,0,0)\right|}\right), \tag{9}$$

where

$$\alpha = \left|\left\langle -1,\frac{1}{2},\frac{1}{2},0\middle|d_\uparrow^\dagger\middle|-2,0,0,0\right\rangle\right|^2 = 1/2,$$

$$\beta = \left|\langle 0,0,0,0|d_\downarrow^\dagger\left|-1,\frac{1}{2},\frac{1}{2},0\right\rangle\right|^2 = \frac{(4t_d+U+\sqrt{16t_d^2+U^2})^2}{8[16t_d^2+U(U+\sqrt{t_d^2+U^2})]}. \tag{10}$$

The factor of $0.182U$ in Eq. (8) is the effective bandwidth. The same effective bandwidth was used to obtain T_K of the Anderson model in the regime $U<D$.[23,26]

B. Spectral densities

We observed that the spectral density calculation using the conventional NRG approach[27] fails for our model. The spectral densities manifest spurious discontinuities, and the normalization sum rule is violated for some choices of model parameters (Fig. 5). This happens because at the early stages of the NRG iteration the lowest-energy state does not yet correspond to the true ground state. We found that we obtain correct results using the density-matrix (DM) NRG

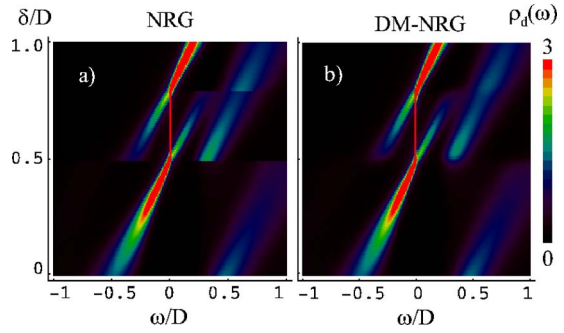

FIG. 6. (Color online) Zero-temperature spectral density $\rho_d(\omega)$ sweeps for $t_d/D=0.3$. (a) Spectral density calculated using the conventional NRG approach. (b) Spectral density calculated using the density-matrix NRG approach. Note that the vertical line, representing the Kondo peak, has been artificially broadened. Its true width is given by T_K.

technique,[24] which remedies the shortcomings of the conventional approach. We succeeded in implementing this technique with eigenstates defined within subspaces with well-defined occupation Q and total spin S, as opposed to well-defined occupation and total spin component S_z (see the Appendix). The improvement in numerical efficiency is sufficient to enable consideration of more complex systems, such as the double quantum dot.

In Fig. 6 we present sweeps of $\rho_d(\omega)$ calculated using both approaches. In vast regions of the plot the results are in perfect agreement. The differences appear for those values of δ where the ground state changes. Three characteristic spectral density curves calculated using the DM-NRG technique are shown in Fig. 7.

Features in the spectral density sweeps can be easily interpreted using eigenvalue diagram in Fig. 3. At low temperatures and for constant δ, the spectral density $A(\omega)$ will be high whenever the energy difference $\Delta E=E_1-E_0$ between the ground state (0) and an excited state (1) is equal to $+\omega$ (particle excitations, $Q_1=Q_0+1$, $S_1=S_0\pm\frac{1}{2}$) or to $-\omega$ (hole excitations, $Q_1=Q_0-1$, $S_1=S_0\pm\frac{1}{2}$). At $\delta=0$ two broad peaks

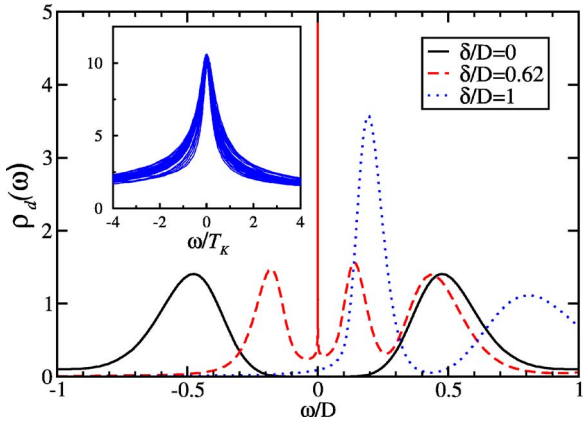

FIG. 7. (Color online) Three zero-temperature spectral densities $\rho_d(\omega)$ for $t_d/D=0.3$: at the particle-hole symmetric point $\delta/D=0$, in the Kondo regime $\delta/D=0.62$, and in the empty-orbital regime $\delta/D=1$. Inset: scaling of spectral densities $\rho_d(\omega/T_K)$ in the Kondo region $0.52<\delta<0.76$. Parameters are as in Fig. 2.

are seen located symmetrically at $\omega\sim\pm\delta_1$ (see Figs. 6 and 7, at $\delta/D=0$). At this point the model is particle-hole symmetric and therefore $E(Q,S,r)=E(-Q,S,r)$ for all Q,S,r. Consequently, the spectrum is also symmetric, $\rho_d(\omega)=\rho_d(-\omega)$. With increasing δ, the particle excitation energy $E(1,\frac{1}{2},0)-E(0,0,0)$ increases and the corresponding peak quickly washes out. The hole excitation energy $E(-1,\frac{1}{2},0)-E(0,0,0)$ decreases and the peak gains weight.

At $\delta=\delta_1$, $E(0,0,0)=E(-1,\frac{1}{2},0)$ (point A in Fig. 3) and the system enters the Kondo regime: a sharp many-body resonance appears which remains pinned at the Fermi level throughout the Kondo region (see Figs. 6 and 7, at $\delta/D=0.62$). The Kondo effect occurs whenever the ground state is a doublet, $S=1/2$, and there are excited states with $S'=0,1$, $Q'=Q\pm1$. We recognize such regions by characteristic triangular level crossings in the eigenvalue diagram, one of which is marked as triangle ABC in Fig. 3. The high-energy peaks at $\omega=E(0,0,0)-E(-1,\frac{1}{2},0)>0$ and $\omega=E(-1,\frac{1}{2},0)-E(-2,0,0)<0$ in the spectral density are also characteristic: they correspond to particle and hole excitations that are at the heart of the Kondo effect.

In the case of the DQD we also see additional structure for $\delta_1<\delta<\delta_2$: a broad peak at $\omega=E(0,1,0)-E(-1,\frac{1}{2},0)$ which corresponds to virtual triplet excitations from the ground state. These excitations could also be taken into account in the calculation of the effective exchange interaction, Eq. (9); however, due to their high energy, they only lead to an exponentially small renormalization of the Kondo temperature, which may be neglected.

In the inset of Fig. 7 we show scaling of Kondo peaks versus ω/T_K. In the case of perfect scaling, all curves should exactly overlap. However, Kondo temperatures of different peaks differ by almost four orders of magnitudes, as seen in Fig. 4(b). Moreover, Kondo peaks become asymmetric near the edges of the Kondo region—i.e., for $\delta\gtrsim\delta_1$ and $\delta\lesssim\delta_2$. Note also that for each point in Fig. 4(b) there is a respective spectral density presented in the inset of Fig. 7.

C. Effect of the on-site-energy splitting

In real double-quantum-dot systems, it is difficult to produce dots and electrodes with identical properties. In particular, it is not easy to achieve equal on-site energies $\delta_d=\delta_a=\delta$ for a wide range of parameters δ. Therefore it is necessary to study the robustness of the physical regimes with respect to the splitting of the on-site energies.

We now generalize slightly our model to allow for unequal on-site energies by introducing a new parameter κ, so that on-site energies are $\delta_d=\delta+\kappa$ and $\delta_a=\delta-\kappa$. The DQD part of the Hamiltonian is now

$$H_0=(\delta+\kappa)(n_d-1)+(\delta-\kappa)(n_a-1)-t_d\sum_\sigma(d_\sigma^\dagger a_\sigma+a_\sigma^\dagger d_\sigma)$$
$$+\frac{U}{2}(n_d-1)^2+\frac{U}{2}(n_a-1)^2. \quad (11)$$

Only $\kappa>0$ has to be considered, because $H_0(\delta,-\kappa)\to H_0(-\delta,\kappa)$ when particle-hole transformation $d_\mu^\dagger\to d_\mu, a_\mu^\dagger\to -a_\mu$ is performed.

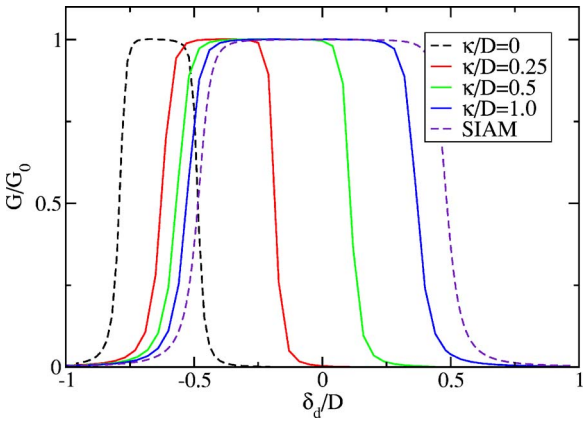

FIG. 8. (Color online) Conductance as a function of gate-voltage δ_d for different gate-voltage asymmetries κ. The label SIAM corresponds to results for conductance of the corresponding single-impurity Anderson model. The temperature is $T/D=10^{-9}$.

By diagonalization H_0 exactly, we find that the effect of κ is to shift states while the general eigenvalue structure is maintained and is similar to that shown in Fig. 3. We therefore still expect to see two Kondo peaks as δ is swept for a constant κ.

In the limit of large κ and for δ such that $\delta_d \sim 0$ and $\delta_a \to \pm\infty$, the side-coupled dot becomes irrelevant and we recover the familiar single-impurity Anderson model with conduction plateau in the region $-U/2 < \delta_d < U/2$ with T_K given by Eq. (8) with

$$\rho_0 J = \frac{2\Gamma}{\pi}\left(\frac{1}{|\delta_d - U/2|} + \frac{1}{|\delta_d + U/2}\right). \tag{12}$$

This scenario is corroborated by NRG calculations (Fig. 8). The approach to the limit can be determined using expressions (8) and (9), with κ-dependent $\alpha(\kappa)$, $\beta(\kappa)$, and $E_1(\kappa), E_2(\kappa)$. The result is shown in Fig. 9(a). The κ dependence is nonmonotonic, which can be traced to the nonmonotonic behavior of the coefficient $\beta(\kappa)$. At $\kappa/D=1$ the

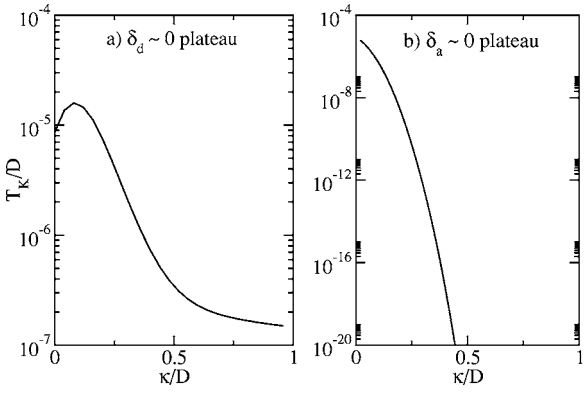

FIG. 9. Kondo temperature as a function of κ for (a) the Kondo plateau at $\delta_d \sim 0$ and (b) the Kondo plateau at $\delta_a \sim 0$. In both cases we calculate the Kondo temperature in the middle of the plateau, where T_K is lowest. Parameters are $U/D=1$, $\Gamma/D=0.03$, and $t_d/D=0.3$.

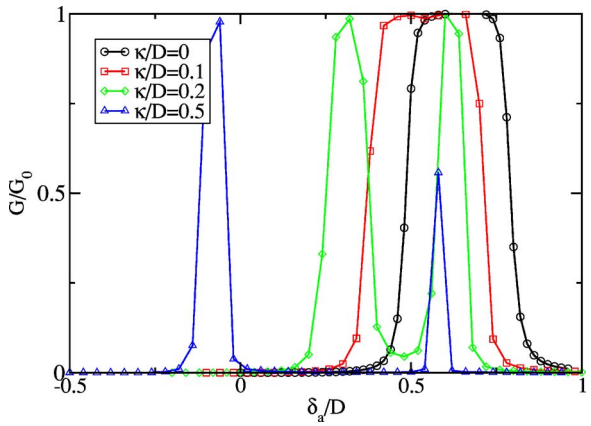

FIG. 10. (Color online) Conductance as a function of gate-voltage δ_a for different gate-voltage asymmetries κ. The temperature is fixed to $T/D=10^{-9}$ for all κ.

asymptotic value $T_K/D=1.04\times10^{-7}$ is nearly reached.

In the limit of large κ, but for δ such that $\delta_a \sim 0$ and $\delta_d \to \pm\infty$, the embedded dot will be either fully occupied or empty with very little charge fluctuations, while the side-coupled dot will maintain $S=1/2$ spin moment. This moment will be screened, but due to the suppression of the virtual electron hopping through the dot d, the corresponding Kondo temperature rapidly drops with increasing κ [Fig. 9(b)]. Keeping the temperature constant and increasing κ, the Kondo plateau in the region $-U/2 < \delta_a < U/2$ will therefore quickly evolve into two peaks separated by a Coulomb blockade valley and for very large κ it will not conduct at all. This prediction can also be verified using NRG (Fig. 10).

IV. WEAK INTERDOT COUPLING

A. Conductance and correlation functions

We now turn to the limit when $t_d \to 0$. Unless otherwise specified, we choose the effective temperature T to be finite—i.e., $T \sim 10^{-9}D$, since calculations at much lower temperatures would be experimentally irrelevant. In this case one naively expects to obtain essentially identical conductance as in the single-dot case. As δ decreases below $\delta \sim U/2$, G/G_0 indeed follows result obtained for the single-dot case as shown in Fig. 11(a). In the case of DQD's, however, a sharp Fano resonance appears at $\delta=U/2$. This resonance coincides with the sudden jump in S, $\langle n\rangle$, as well as with the spike in Δn^2, as shown in Figs. 11(b)–11(d), respectively. Fano resonance is a consequence of a sudden charging of the nearly decoupled dot a, as its level ϵ crosses the chemical potential of the leads—i.e., at $\epsilon=0$. Meanwhile, the electron density on the dot d remains a smooth function of δ, as seen from $\langle n_d\rangle$ in Fig. 11(c). With increasing t_d, the width of the resonance increases, as shown for $t_d/D=0.01$ in Fig. 11(f). For $t_d \gtrsim 0.1$, the resonance merges with the Kondo plateau and disappears [see Fig. 2(a)].

The resonance at $\delta \sim U/2$ can be explained using a simple semianalytical model. For $t_d=0$, we write the exact Green's function of the impurity d at $\omega=0$ as $\mathcal{G}_d^0 = 1/(i\Gamma - \Gamma\cot\phi)$,[28] where ϕ is the scattering phase shift for single impurity

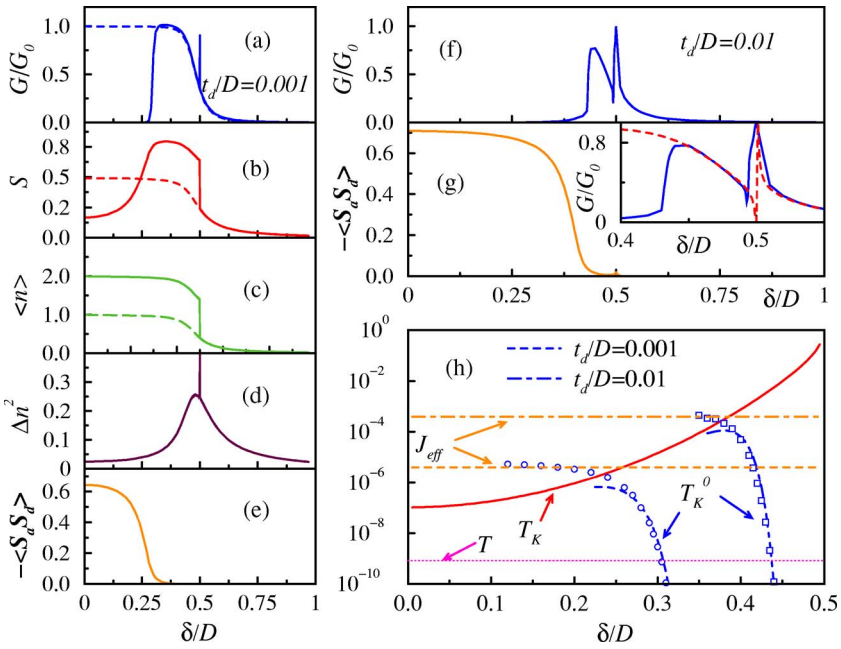

FIG. 11. (Color online) Conductance and correlation functions at $t_d/D=0.001$ (a)–(e), $t_d/D=0.01$ (f) and (g), and a blow-up of (f) in the inset of (g). Dashed lines in (a) represent G/G_0 and (b) S of a single quantum dot with otherwise identical parameters. Dashed line in (c) represents $\langle n_d\rangle$ of DQD, and finally dashed line in the inset of (g) represents the semianalytical model described in the text. In (h) a schematic plot of different temperatures and interactions is presented as explained in the text. NRG values of the gap in $\rho_d(\omega)$ at $\omega=0$ and $T\ll T_K^0$ are presented with open circles and squares for $t_d/D=0.001$ and 0.01, respectively. Values of J_{eff} and analytical results of T_K^0 are presented as dashed and dot-dashed lines for $t_d/D=0.001$ and 0.01, respectively. For analytical estimates of T_K^0 different values of $\alpha=2.2$ and 1.3, respectively, were used. Other parameters of the model are $\Gamma/D=0.03$, $U/D=1$.

model that we calculate using NRG. The side-coupled dot is taken into account using perturbation theory. We obtain full Green's function from the Dyson's equation

$$\mathcal{G}_d = \mathcal{G}_d^0/(1 - t_d^2 \mathcal{G}_a^0 \mathcal{G}_d^0). \tag{13}$$

For the Fano resonance at $\epsilon=\delta-U/2\sim 0$, we keep only the low-energy pole in the Green's function,

$$\mathcal{G}_a^0(\omega) \approx \frac{z}{\omega - \epsilon + i\eta}, \tag{14}$$

where $z=\frac{1}{2}$ for $\epsilon<0$ and $z=1$ for $\epsilon>0$. The conductance is

$$G = G_0 \frac{2\Gamma^2 \epsilon^2 \sin^2\phi}{z^2 t_d^4 + 2\Gamma^2\epsilon^2 - z^2 t_d^4 \cos(2\phi) - 2z t_d^2 \epsilon\Gamma \sin(2\phi)}. \tag{15}$$

Results of the NRG calculation are compared to the prediction from Eq. (15) in the inset of Fig. 11(g). We see that the general features are adequately described, but there are subtle differences due to nonperturbative electron correlation effects. The numerically calculated Fano resonance is wider than the semianalytical prediction, and G/G_0 does not drop to zero. In particular, from Eq. (15) it follows that $G=0$ at $\delta=U/2$ ($\epsilon=0$) and $G=G_0$ at $\delta=U/2+t_d^2\tan\phi/\Gamma$. This is not corroborated by NRG results, which show maximal conductance at $\delta=U/2$.

We now return to the description of the results presented in Fig. 11(a) in the regime where $\delta<U/2$. As δ further decreases, the system enters a regime of the two-stage Kondo effect.[17] This region is defined by $J_{\text{eff}}<T_K$ [see also Fig. 11(h)], where T_K is the Kondo temperature, approximately given by the single-quantum-dot Kondo temperature, Eq. (8), with

$$\rho_0 J = \frac{2\Gamma}{\pi}\left(\frac{1}{|\delta - U/2|} + \frac{1}{|\delta + U/2|}\right). \tag{16}$$

Just below $\delta<U/2$, T falls in the interval, given by $T_K^0 \ll T \ll T_K$, where

$$T_K^0 \sim T_K \exp(-\alpha T_K/J_{\text{eff}}) \tag{17}$$

denotes the lower Kondo temperature, corresponding to the gap in the spectral density $\rho_d(\omega)$ at $\omega=0$ and α is of the order of 1 (Ref. 17). Note that NRG values of the gap in $\rho_d(\omega)$ (open circles and squares), calculated at $T\ll T_K^0$, follow analytical results for $T_K^0(\delta)$ when $J_{\text{eff}}<T_K$ [see Fig. 11(h)], while in the opposite regime—i.e., for $J_{\text{eff}}>T_K$—they approach J_{eff}.

As shown in Fig. 11(a) for $0.3D\lesssim\delta<U/2$, G/G_0 calculated at $T=10^{-9}D$ follows results obtained in the single-quantum-dot case and approaches the value 1. The spin quantum number S in Fig. 11(b) reaches the value $S\sim 0.8$, consistent with the result obtained for a system of two decoupled spin-1/2 particles, where $\langle\hat{\mathbf{S}}^2\rangle=3/2$. This result is also in agreement with $\langle n\rangle\sim 2$ and the small value of the spin-spin correlation function $\langle \mathbf{S}_a\cdot\mathbf{S}_d\rangle$, presented in Figs. 11(c) and 11(e), respectively.

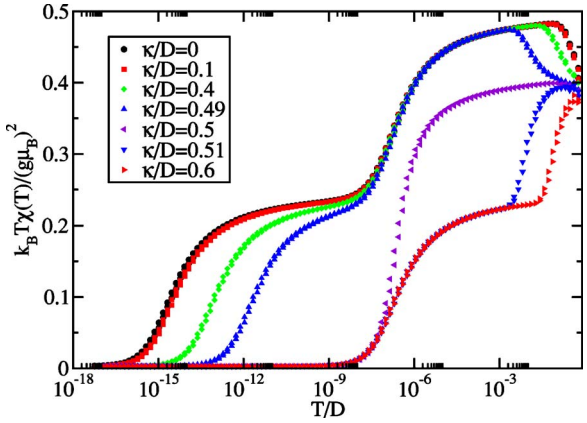

FIG. 12. (Color online) Dynamic magnetic susceptibility $k_BT\chi(T)/(g\mu_B)^2$ for different κ. Parameters are $U/D=1$, $\Gamma/D=0.03$, $t_d/D=8\times10^{-5}$, and $\delta/D=0$. These calculations were performed using a different NRG discretization scheme (Ref. 29) with $\Lambda=4$ and keeping 600 states.

With further decreasing of δ, G/G_0 suddenly drops to zero at $\delta\lesssim 0.3D$. This sudden drop is approximately given by $T\lesssim T_K^0(\delta)$ [see Figs. 11(a) and 11(h)]. At this point the Kondo hole opens in $\rho_d(\omega)$ at $\omega=0$, which in turn leads to a drop in the conductivity. The position of this sudden drop in terms of δ is rather insensitive to the chosen T, as apparent from Fig. 11(h).

Below $\delta\lesssim 0.25D$, which corresponds to the condition $J_{\text{eff}}\sim T_K(\delta)$, also presented in Fig. 11(h), the system crosses over from the two-stage Kondo regime to a regime where spins on DQD's form a singlet. In this case S decreases and $\langle \mathbf{S}_a\cdot\mathbf{S}_d\rangle$ shows strong antiferromagnetic correlations, Figs. 11(b) and 11(e). The lowest energy scale in the system is J_{eff}, which is supported by the observation that the size of the gap in $\rho_d(\omega)$ [open circles in Figs. 11(h)] is approximately given by J_{eff}. The main difference between $t_d/D=0.001$ and $t_d/D=0.01$ comes from different values of $J_{\text{eff}}=4t_d^2/U$. Since in the latter case J_{eff} is larger, the system enters the AFM singlet regime at much larger values of δ, as can be seen from comparison of Figs. 11(g) and 11(f). Consequently, the regime of enhanced conductance shrinks.

B. Effect of the on-site-energy splitting

We again explore the effect of unequal on-site energies. Unlike in Sec. III C, we now introduce the asymmetry so that only the level a is shifted by the parameter κ: $\delta_d=\delta$ and $\delta_a=\delta+\kappa$. We are mainly interested in the parameter range where for $\kappa=0$ the system exhibits the two-stage Kondo effect.

This study will be conducted by computing the impurity susceptibility

$$\chi_{\text{imp}}(T)=\frac{(g\mu_B)^2}{k_BT}(\langle S_z^2\rangle-\langle S_z^2\rangle_0), \tag{18}$$

where the first expectation value refers to the system with the double quantum dot, while the second refers to the system without dots. In traces of $T\chi_{\text{imp}}$, the two-stage Kondo effect manifests as two successive decreases of the susceptibility, at $T\sim T_K$ from around 0.5 to 0.25 and at $T\sim T_K^0$ from around 0.25 to 0.[17] We now investigate how this behavior changes when $\kappa\neq 0$ by comparing temperature-dependent susceptibilities calculated for a range of parameters κ.

We find that the two-stage Kondo effect is robust against $\kappa\neq 0$ perturbation. In fact, it survives until $\kappa=U/2$ (see Fig. 12). For $\kappa<U/2$ the main effect of κ is to reduce the lower Kondo temperature T_K^0. For $\kappa>U/2$, dot a becomes irrelevant at low temperatures and dot d is in the usual Kondo regime.

The transition from $\kappa<U/2$ to $\kappa>U/2$ is continuous despite a rather abrupt change in χ_{imp} caused by a rapid change in occupation of dot a that occurs with increasing κ on an energy scale proportional to t_d^2. For $\kappa=U/2$, $\epsilon_a=\delta_a-U/2=0$ and the side-coupled dot is in the valence-fluctuation regime. For two uncoupled dots, one in the local-moment regime and the other in the valence-fluctuation regime, the magnetic moment $k_BT\chi/(g\mu_B)^2$ is expected to be $1/4+1/6=5/12$. At high temperatures, χ is indeed in the vicinity of this value.

V. CONCLUSIONS

In this paper we have explored different regimes of the side-coupled DQD. When quantum dots are *strongly coupled*, wide regions of enhanced, nearly unitary conductance exist due to the underlying Kondo physics. Analytical estimates for their positions and widths, as well as for the corresponding Kondo temperatures, are given and numerically verified. When two electrons occupy a DQD, the conductance is zero due to the formation of a spin-singlet state which is effectively decoupled from the leads. In this regime most physical properties of the coupled DQD's can be predicted using the eigenvalue diagram of the isolated DQD system. This happens because energy separations of different DQD states are much larger than the Kondo temperature. Introducing the on-site-energy splitting between DQD's induces new, even though not unexpected, effects within the Kondo regime. With increasing level splitting, the Kondo plateau is expanded when the level of the embedded dot is kept near the local particle-hole limit. In the other case, when, in contrast, the level of the side-coupled dot is kept near the particle-hole limit, Kondo plateau splits at finite T due to abrupt decrease of T_K with increasing level splitting.

When quantum dots are *weakly coupled* Fano resonance appears in the valence-fluctuation regime. Its width is enhanced as a consequence of interactions which should facilitate experimental observation. Unitary conductance exists when two electrons occupy a DQD due to a two-stage Kondo effect as long as the temperature of the system is well below T_K and above T_K^0. The experimental signature of the two-stage Kondo effect in the weakly coupled regime should materialize through the interdot-coupling sensitive width of the enhanced conductance versus gate voltage. Experimental observation of the two-stage Kondo effect would require no external magnetic field as used in Ref. 7. The interdot-coupling strength can be experimentally varied using gate electrodes.[1–4]

ACKNOWLEDGMENTS

The authors acknowledge useful discussions with A. Ramšak, C.D. Batista, and S.A. Trugman and the financial support of the SRA under Grant No. P1-0044.

APPENDIX: DENSITY-MATRIX NRG IN A (Q,S) SUBSPACE BASIS

The density-matrix numerical renormalization group[24] was originally implemented for a NRG iteration that uses subspaces with well-defined charge Q and spin projection S_z and it was used to determine the effect of magnetic field on spin-projected spectral densities. In the absence of a magnetic field, when rotational invariance in the spin space is recovered, it is advantageous to use subspaces with well-defined charge Q and spin S, which leads to greatly enhanced numerical efficiency.

Here we show how the DM-NRG can be implemented in a (Q,S) subspace basis in the case of a single conduction channel.

The density matrix at the last iteration step (estimated using the truncated basis) is

$$\rho = \frac{1}{Z}\sum_{QSS_z\omega} \exp(-\beta E_{QS\omega})|QSS_z\omega\rangle\langle QSS_z\omega|, \tag{A1}$$

where ω enumerates different states in each (Q,S) subspace and the grand-canonical statistical sum Z is

$$Z = \mathrm{Tr}[\exp(-\beta H)] = \sum_{QSS_z\omega} \exp(-\beta E_{QS\omega}). \tag{A2}$$

Unitary transformation of states from the Nth to the $(N+1)$th stage is

$$|QSS_z\omega\rangle_{N+1} = \sum_{r\alpha} U_{QS}(\omega|r\alpha)|QSS_zr\alpha\rangle_{N+1}, \tag{A3}$$

where U_{QS} are the corresponding unitary transformation matrices obtained during the diagonalization step of the NRG and the $|QSS_z\alpha r\rangle_{N+1}$ states are defined as[23]

$$|QSS_zr1\rangle_{N+1} = |Q+1,SS_zr\rangle_N,$$

$$|QSS_zr2\rangle_{N+1} = uf^\dagger_{(N+1)\uparrow}\left|Q,S-\frac{1}{2},S_z-\frac{1}{2},r\right\rangle_N + vf^\dagger_{(N+1)\downarrow}\left|Q,S-\frac{1}{2},S_z+\frac{1}{2},r\right\rangle_N,$$

$$|QSS_zr3\rangle_{N+1} = wf^\dagger_{(N+1)\uparrow}\left|Q,S+\frac{1}{2},S_z-\frac{1}{2},r\right\rangle_N + yf^\dagger_{(N+1)\uparrow}\left|Q,S+\frac{1}{2},S_z+\frac{1}{2},r\right\rangle_N,$$

$$|QSS_zr4\rangle_{N+1} = f^\dagger_{(N+1)\uparrow}f^\dagger_{(N+1)\downarrow}|Q-1,SS_zr\rangle_N|\uparrow\downarrow\rangle, \tag{A4}$$

where $f^\dagger_{(N+1)\sigma}$ is the creation operator for electrons on the $(N+1)$th site of the "hopping Hamiltonian" and u, v, w, and y are the Clebsch-Gordan coefficients:

$$u = \left(\frac{S+S_z}{2S}\right)^{1/2},$$

$$v = \left(\frac{S-S_z}{2S}\right)^{1/2},$$

$$w = -\left(\frac{S-S_z+1}{2S+2}\right)^{1/2},$$

$$y = \left(\frac{S+S_z+1}{2S+2}\right)^{1/2}.$$

The density matrix in the basis of $|QSS_z\alpha r\rangle_{N+1}$ states is

$$\rho = \sum_{QSS_z\omega} \exp(-\beta E_{QS\omega}) \sum_{r\alpha,r'\alpha'} U_{QS}(\omega|r\alpha)U_{QS}(\omega|r'\alpha') \times |QSS_zr\alpha\rangle\langle QSS_zr'\alpha'|. \tag{A5}$$

We now perform a partial trace over the states on the additional $(N+1)$th site to obtain projector operators defined on the chain of length N. Diagonal projectors (those with $\alpha=\alpha'$) are

$$\mathrm{Tr}_{N+1}(|QSS_zr1\rangle\langle QSS_zr'1|) = |Q+1,SS_zr\rangle_N\langle Q+1,SS_zr'|_N,$$

$$\mathrm{Tr}_{N+1}(|QSS_zr4\rangle\langle QSS_zr'4|) = |Q-1,SS_zr\rangle_N\langle Q-1,SS_zr|_N,$$

$$\mathrm{Tr}_{N+1}(|QSS_zr2\rangle\langle QSS_zr'2|) = u^2\left|Q,S-\frac{1}{2},S_z-\frac{1}{2},r\right\rangle_N\left\langle Q,S-\frac{1}{2},S_z-\frac{1}{2},r'\right|_N + v^2\left|Q,S-\frac{1}{2},S_z+\frac{1}{2},r\right\rangle_N\left\langle Q,S-\frac{1}{2},S_z+\frac{1}{2},r'\right|_N,$$

$$\mathrm{Tr}_{N+1}(|QSS_zr3\rangle\langle QSS_zr3|) = w^2\left|Q,S+\frac{1}{2},S_z-\frac{1}{2},r\right\rangle_N\left\langle Q,S+\frac{1}{2},S_z-\frac{1}{2},r'\right|_N + y^2\left|Q,S+\frac{1}{2},S_z+\frac{1}{2},r\right\rangle_N\left\langle Q,S+\frac{1}{2},S_z+\frac{1}{2},r'\right|_N. \tag{A6}$$

The out-of-diagonal $\alpha=2,\alpha'=3$ terms give zero when summed over

$$\sum_{S_z=-S}^{S}\mathrm{Tr}_{N+1}|QSS_zr2\rangle\langle QSS_zr'3| = \sum_{S_z=-S+1}^{S}\left(-\sqrt{\frac{(S+S_z)(S-S_z+1)}{2S(2S+2)}} + \sqrt{\frac{(S-S_z+1)(S+S_z)}{2S(2S+2)}}\right) \times \left|Q,S-\frac{1}{2},S_z-\frac{1}{2},r\right\rangle_N\left\langle Q,S+\frac{1}{2},S_z-\frac{1}{2},r'\right|_N = 0, \tag{A7}$$

where we took into account that $v_{SS}=0$ and $u_{S,-S}=0$ in order to expand the range of the summation index S_z. Similarly we show that $\alpha=3$ and $\alpha'=2$ terms are dropped.

The $\alpha=\alpha'=2$ terms can be simplified after summing over S_z:

$$\sum_{S_z=-S}^{S} \mathrm{Tr}_{N+1}(|QSS_zr2\rangle\langle QSS_zr'2|)$$
$$= \sum_{S_z=-S+1}^{S} (u^2_{SS_z}+v^2_{S,S_z-1}) \times \left|Q,S-\frac{1}{2},S_z-\frac{1}{2},r\right\rangle_N \left\langle Q,S-\frac{1}{2},S_z-\frac{1}{2},r'\right|_N$$
$$= \frac{2S+1}{2S} \sum_{S_z=-(S-1/2)}^{+(S-1/2)} \left|Q,S-\frac{1}{2},S_z\right\rangle_N \left\langle Q,S-\frac{1}{2},S_z,r'\right|_N. \quad \text{(A8)}$$

The spin multiplicity of $(QS)_{N+1}$ space is $2S+1$, while the spin multiplicity of $\left(Q,S-\frac{1}{2}\right)_N$ is $2S$. The factor $(2S+1)/(2S)$ is therefore merely a normalization factor. In the last line we emphasized that in the N-site space the S_z runs over all permissible values for spin $S-\frac{1}{2}$.

By analogy we show that the $\alpha=\alpha'=3$ terms also simplify:

$$\sum_{S_z=-S}^{S} \mathrm{Tr}_{N+1}(|QSS_zr3\rangle\langle QSS_zr3|)$$
$$= \frac{2S+1}{2S+2} \sum_{S_z=-(S+1/2)}^{S+1/2} \left|Q,S+\frac{1}{2},S_z,r\right\rangle_N \left\langle Q,S+\frac{1}{2},S_z,r'\right|_N. \quad \text{(A9)}$$

Again, the spin multiplicity of the $\left(Q,S+\frac{1}{2}\right)_N$ space is $2S+2$ and the factor $(2S+1)/(2S+2)$ takes care of the correct normalization.

Nonzero partial traces of projector operators are therefore

$$\sum_{S_z} \mathrm{Tr}_{N+1}|QSS_zr\alpha\rangle\langle QSS_zr'\alpha'| = \delta_{\alpha\alpha'}c_\alpha(S)\sum_{S_{z\alpha}} |Q_\alpha S_\alpha S_{z\alpha}r\rangle_N\langle Q_\alpha S_\alpha S_{z\alpha}r'|_N, \quad \text{(A10)}$$

with $c_1=c_4=1$, $c_2=(2S+1)/2S$, $c_3=(2S+1)/(2S+2)$, $Q_1=Q+1$, $Q_2=Q_3=Q$, $Q_4=Q-1$, $S_1=S_4=S$, $S_2=S-\frac{1}{2}$, $S_3=S+\frac{1}{2}$, and the corresponding $S_{z\alpha}$ ranges over all possible values for a given S_α. The reduced density matrix remains diagonal in its (Q,S) subspace index.

In general we therefore have

$$\rho^{N+1}_{\mathrm{reduced}} = \sum_{QSS_z}\sum_{\omega\omega'} C^{QS,N+1}_{\omega\omega'}|QSS_z\omega\rangle\langle QSS_z\omega'|$$
$$= \sum_{QS}\sum_{\omega\omega'} C^{QS,N+1}_{\omega\omega'} \sum_{r\alpha,r'} U_{QS}(\omega|r\alpha)U_{QS}(\omega'|r'\alpha)c_\alpha(S) \times \sum_{S_{z\alpha}} |Q_\alpha S_\alpha S_{z\alpha}r\rangle_N\langle Q_\alpha S_\alpha S_{z\alpha}r'|_N. \quad \text{(A11)}$$

This is to be comapred with

$$\rho^{N}_{\mathrm{reduced}} = \sum_{QSS_z}\sum_{rr'} C^{QS,N}_{rr'}|QSS_zr\rangle\langle QSS_zr'|. \quad \text{(A12)}$$

We finally obtain the recursion relation for calculation of coefficients $C^{QS,N}_{rr'}$ in the reduced density matrix:

$$C^{QS,N}_{rr'} = \sum_{\omega\omega'} C^{Q-1,S,N+1}_{\omega\omega'} U_{Q-1,S}(\omega|r1)U_{Q-1,S}(\omega'|r'1) + \sum_{\omega\omega'} C^{Q+1,S,N+1}_{\omega\omega'} U_{Q+1,S}(\omega|r4)U_{Q+1,S}(\omega'|r'4) + \frac{2S+2}{2S+1}\sum_{\omega\omega'} C^{Q,S+1/2,N+1}_{\omega\omega'} U_{Q,S+1/2} \times(\omega|r2)U_{Q,S+1/2}(\omega'|r'2) + \frac{2S}{2S+1}\sum_{\omega\omega'} C^{Q,S-1/2,N+1}_{\omega\omega'} U_{Q,S-1/2} \times(\omega|r3)U_{Q,S-1/2}(\omega'|r'3). \quad \text{(A13)}$$

This is the main result of the derivation. Using known $U_{Q,S}$ matrices, recursion in Eq. (A13) is applied after the first NRG run to calculate reduced density matrices for all chain lengths. In another NRG run, the spectral density functions are then calculated with respect to the reduced density matrices:

$$A^N_{d\sigma}(\omega) = \sum_{ijm} (\langle j|d^\dagger_\sigma|m\rangle\langle j|d^\dagger_\sigma|i\rangle\rho^{\mathrm{reduced}}_{im} + \langle i|d^\dagger_\sigma|m\rangle \times\langle j|d^\dagger_\sigma|m\rangle\rho^{\mathrm{reduced}}_{ji})\delta(\omega-(E_j-E_m)). \quad \text{(A14)}$$

[1] H. Jeong, A. M. Chang, and M. R. Melloch, Science **293**, 2221 (2001).

[2] N. J. Craig, J. M. Taylor, E. A. Lester, C. M. Marcus, M. P. Hanson, and A. C. Gossard, Science **304**, 565 (2004).

[3] A. W. Holleitner, R. H. Blick, A. K. Huttel, K. Eberl, and J. P. Kotthaus, Science **297**, 70 (2002).

[4] J. C. Chen, A. M. Chang, and M. R. Melloch, Phys. Rev. Lett. **92**, 176801 (2004).

[5] W. Hofstetter and H. Schoeller, Phys. Rev. Lett. **88**, 016803 (2003).

[6] W. Hofstetter and G. Zarand, Phys. Rev. B **69**, 235301 (2004).

[7] W. G. van der Wiel, S. De Franceschi, J. M. Elzerman, S. Tarucha, L. P. Kouwenhoven, J. Motohisa, F. Nakajima, and T. Fukui, Phys. Rev. Lett. **88**, 126803 (2002).

[8] G. Granger, M. A. Kastner, I. Radu, M. P. Hanson, and A. C. Gossard, Phys. Rev. B **72**, 165309 (2005).

[9] K. Kobayashi, H. Aikawa, S. Katsumoto, and Y. Iye, Phys. Rev. Lett. **88**, 256806 (2002).

[10] K. Kobayashi, H. Aikawa, A. Sano, S. Katsumoto, and Y. Iye, Phys. Rev. B **70**, 035319 (2004).
[11] B. R. Bulka and P. Stefanski, Phys. Rev. Lett. **86**, 5128 (2001).
[12] P. Stefanski, A. Tagliacozzo, and B. R. Bulka, Phys. Rev. Lett. **93**, 186805 (2004).
[13] G. A. Lara, P. A. Orellana, J. M. Yanez, and E. V. Anda, Solid State Commun. **136** (6), 323 (2005); A. A. Aligia and L. A. Salguero, Phys. Rev. B **70**, 075307 (2004).
[14] T.-S. Kim and S. Hershfield, Phys. Rev. B **63**, 245326 (2001).
[15] V. M. Apel, M. A. Davidovich, E. V. Anda, G. Chiappe, and C. A. Busser, Eur. Phys. J. B **40**, 365 (2004).
[16] K. Kang, S. Y. Cho, J.-J. Kim, and S.-C. Shin, Phys. Rev. B **63**, 113304 (2001).
[17] P. S. Cornaglia and D. R. Grempel, Phys. Rev. B **71**, 075305 (2005).
[18] M. Vojta, R. Bulla, and W. Hofstetter, Phys. Rev. B **65**, 140405(R) (2002).
[19] L. I. Glazman and M. E. Raikh, JETP Lett. **47**, 452 (1988).
[20] Y. Meir and N. S. Wingreen, Phys. Rev. Lett. **68**, 2512 (1992).
[21] K. G. Wilson, Rev. Mod. Phys. **47**, 773 (1975).
[22] T. A. Costi, Phys. Rev. B **64**, 241310(R) (2001).
[23] H. R. Krishna-murthy, J. W. Wilkins, and K. G. Wilson, Phys. Rev. B **21**, 1003 (1980).
[24] W. Hofstetter, Phys. Rev. Lett. **85**, 1508 (2000).
[25] A. C. Hewson, *The Kondo Problem to Heavy Fermions* (Cambridge University Press, Cambridge, England, 1993).
[26] F. Haldane, J. Phys. C **11**, 5015 (1978).
[27] T. A. Costi, A. C. Hewson, and V. Zlatic, J. Phys.: Condens. Matter **6**, 2519 (1994).
[28] D. C. Langreth, Phys. Rev. **150**, 516 (1966).
[29] V. L. Campo and L. N. Oliveira, Phys. Rev. B **72**, 104432 (2005).